Biofabrication

PAPER

A handheld bioprinter for multi-material printing of complex constructs

Erik Pagan[1], Evan Stefanek[1], Amir Seyfoori[1], Mahmood Razzaghi[1], Behnad Chehri[1], Ali Mousavi[2,3,4], Pietro Arnaldi[1,8], Zineb Ajji[2,3,4], Daniela Ravizzoni Dartora[3,5], Seyed Mohammad Hossein Dabiri[1], Anne Monique Nuyt[3,5], Ali Khademhosseini[6], Houman Savoji[2,3,4] and Mohsen Akbari[1,6,7,*]

[1] Laboratory for Innovations in Microengineering (LiME), Department of Mechanical Engineering, University of Victoria, Victoria BC V8P 5C2, Canada
[2] Institute of Biomedical Engineering, Department of Pharmacology and Physiology, Faculty of Medicine, University of Montreal, Montreal QC H3T 1J4, Canada
[3] Research Center, Centre Hospitalier Universitaire Sainte-Justine, Montreal QC H3T 1C5, Canada
[4] Montreal TransMedTech Institute, Montreal QC H3T 1C5, Canada
[5] Department of Pediatrics, Faculty of Medicine, University of Montreal, Montreal QC H3T 1J4, Canada
[6] Terasaki Institute for Biomedical Innovation, Los Angeles CA 90064, United States of America
[7] School of Biomedical Engineering, University of British Columbia, Vancouver BC V6T 1Z3, Canada
[8] Department of Informatics, Bioengineering, Robotics and Systems Engineering (DIBRIS), University of Genoa, Via All' Opera Pia 13, Genoa 16145, Italy
* Author to whom any correspondence should be addressed.

E-mail: makbari@uvic.ca

Keywords: bioprinting, *in situ* printing, bioinks, drug delivery, cell delivery

Supplementary material for this article is available online

OPEN ACCESS

RECEIVED
6 December 2022

REVISED
16 February 2023

ACCEPTED FOR PUBLICATION
14 March 2023

PUBLISHED
2 May 2023

Abstract

In situ bioprinting—the process of depositing bioinks at a defected area, has recently emerged as a versatile technology for tissue repair and restoration *via* site-specific delivery of pro-healing constructs. The ability to print multiple materials *in situ* is an exciting approach that allows simultaneous or sequential dispensing of different materials and cells to achieve tissue biomimicry. Herein, we report a modular handheld bioprinter that deposits a variety of bioinks *in situ* with exquisite control over their physical and chemical properties. Combined stereolithography 3D printing and microfluidic technologies allowed us to develop a novel low-priced handheld bioprinter. The ergonomic design of the handheld bioprinter facilitate the shape-controlled biofabrication of multi-component fibers with different cross-sectional shapes and material compositions. Furthermore, the capabilities of the produced fibers in the local delivery of therapeutic agents was demonstrated by incorporating drug-loaded microcarriers, extending the application of the printed fibers to on-demand, temporal, and dosage-control drug delivery platforms. Also, the versatility of this platform to produce biosensors and wearable electronics was demonstrated via incorporating conductive materials and integrating pH-responsive dyes. The handheld printer's efficacy in generating cell-laden fibers with high cell viability for site-specific cell delivery was shown by producing single-component and multi-component cell-laden fibers. In particular, the multi-component fibers were able to model the invasion of cancer cells into the adjacent tissue.

1. Introduction

Since its inception in the mid-1980s, three-dimensional (3D) printing has emerged as a transformative tool that can benefit and advance medicine by rapidly prototyping medical devices, implants, drug delivery systems, and complex tissues [1]. Notably, engineering artificial tissues from cells, biomaterials, and bioactive molecules has many applications in biology and medicine [2, 3]. These engineered tissues are used to understand disease formation and progression or to develop biological substitutes to repair or replace damaged organs. Lab-grown tissues can also be utilized to develop

humanized *in vitro* models to validate drug safety and efficacy [2, 4]. Accurate deposition of bioinks is typically accomplished by a variety of techniques that include micro-extrusion- [5], droplet- [6], inkjet- [7], microfluidic(-assisted)- [8], and light-based 3D printing [9]. The structural, physical, and biological properties of bioprinted constructs can be controlled through rational design of bioinks and selection of the most suitable printing method(s) to mimic the native tissue function. Indeed, recapitulating the multiscale complexities of tissues requires advanced technologies that involve high-resolution printing of multiple bioinks and creating sophisticated multiluminal structures [10].

Printing tissues in dishes for organ transplantation face a few practical challenges, including considerable processing times, the need for perfusable bioreactors that mimic the *in vivo* environment for tissue maturation, and inadequate mechanical properties of the final construct that impede its manipulation post-fabrication [11]. *In situ* bioprinting—the process of depositing cells and biomaterials directly into the site of injury—can potentially be used to overcome these challenges for some applications. In this approach, cell and bioink deposition can typically be achieved via robotic arms or handheld printers that deliver materials onto the surface. Subsequently, the body itself acts as a bioreactor to mature the tissue/organ. Moreover, because the tissue will be implanted in the body, no further manipulation of the final construct is needed [12]. More recently, handheld bioprinting technologies have been evolving rapidly due to their inherent advantages over both conventional and *in situ* bioprinting. This approach enables direct control over biomaterial deposition, eliminating the requirement for medical imaging to generate a 3D model of the implant. This significantly reduces the amount of equipment required during use and removes the limitations associated with computer-aided control for printing constructs directly on the wound site [13].

In a pioneering study, O'Connell *et al* developed a handheld device consisting of a custom titanium dual-channel collinear (side-by-side) printhead, each connected to a different bioink cartridge powered by a pressure regulator for pneumatic extrusion and a ultraviolet (UV) light source for crosslinking [14]. Their device is capable of generating dual-material, co-linear fibers as well as fibers with dual-material compositional gradients using a gelatin methacryloyl (GelMA)/hyaluronic acid methacrylate (HAMA) based bioink. While this platform was lightweight, small, and allowed for the generation of constructs comprised of up to two materials, it was limited to photocrosslinkable bioinks. Being made with selective laser melded 3D printed titanium, the device's extruder is expensive to fabricate. Furthermore, the group noted that the pressure needed to be constantly adjusted to maintain a constant flow rate due to variations in temperature caused by the heat from the user's hand. Ying *et al* developed a similar portable, handheld bioprinter capable of depositing cell-loaded photocrosslinkable bioink *in situ* [15]. The device was comprised of a 3D-printed compact, handheld syringe pump with an array of UV light-emitting diodes (LEDs) aimed at the tip of the syringe. They demonstrated the ability to print constructs composed of fibroblast cells as well as human umbilical vein endothelial cells embedded in a pore-forming GelMA/poly(ethylene oxide) (PEO) two-phase emulsion bioink with high cell viability. However, this design was limited to generating homogeneous, single-material constructs and was only compatible with photocrosslinkable bioinks. Moreover, having the stepper motor, batteries, and all other electrical and mechanical components enclosed in the device adds a significant amount of size and weight, negatively impacting ergonomics and comfort, thus hindering long-term operation. Duchi and coworkers further developed this platform with the addition of a co-axial printhead which allowed the generation of cell-embedded core/shell GelMA/HAMA bioscaffolds with high cell viability [16]. They also replaced their pressure-driven extrusion mechanism with a mechanical system with two stepper motors acting as syringe pumps mounted directly on the device. While this extrusion mechanism allowed for a constant flow rate, irrespective of the temperature or viscosity of the material, the need for an individual stepper motor for each material also has a significant impact on the size and weight of the device, hindering the possibility of creating more complex printheads with more than two materials. Other groups including Tamayol and Sinha, extended the applications of handheld bioprinters to wound healing [17] and skeletal muscle [18] and achieved remarkable outcomes in animal models.

The ability to print large quantities of bioinks offers the advantage of covering large tissue areas quickly, a feature that is desired for treating large injuries such as burn wounds. To this aim, Hakimi *et al* developed an extrusion-based handheld skin printer capable of *in situ* deposition of biomaterial or skin tissue sheets from a microfluidic cartridge [19]. A stepper motor and onboard syringe pumps were used to control the bioink/crosslinking agent flow rates and deposition speed from the 3D printed microfluidic cartridge. This device enabled conformal printing of spatially-organized inks carrying dermal and epidermal cells into flat and curved surfaces. Additionally, it was compatible with various types of bioinks including alginate, fibrin, collagen type 1, and hyaluronic acid where an ionic or enzymatic crosslinking approach could be adopted to aid the gelation of the cell-laden sheet. Despit exciting results, his technology was limited to either homogeneous, or simple dual-material chemical compositions and rudimental fiber morphologies, not necessarily mimicking the

multicellular and complex tissues found in the body. Moreover, it was only compatible with a narrow range of biomaterials, and required a rigorous fabrication process, all of which restrict their range of applications.

In this work, we proposed a handheld bioprinter capable of depositing multiple materials with precise control over their spatiotemporal physicochemical properties. Multi-material bioprinting is an exciting approach for improving tissue biomimicry during the printing process as this approach enables simultaneous or sequential dispensing of different materials and cells [2, 20]. The handheld bioprinter reported herein is modular and equipped with a mountable light-emitting compartment that facilitates printing photo-crosslinkable bioinks. Further, we have designed a passive temperature control module that maintains the temperature of cartridges for extended periods, allowing for long-term printing of viscous bioinks. Multi-material printing is achieved by means of multi-channel printheads with complex fluidic circuitry that enable creating complex flows of several bioinks in microscale. The versatility afforded by the modular assembly and wide range of configurations of the rapid-prototyped printheads allow for the fabrication of microfibers with diverse compositions and geometries. We showcased the widespread use of this platform by printing multiple cells, drug-releasing meshes, and sensors.

2. Results and discussion

2.1. Modular handheld printer enables depositing fibers with controlled biochemical and biophysical features

We combined high-resolution stereolithography (SLA) 3D printing and microfluidic technologies to develop an inexpensive, modular handheld bioprinting system (figure 1). The device is composed of (i) a printhead made with a high-resolution resin SLA 3D printer, (ii) pneumatic syringe cartridges adapted for hydraulic extrusion, (iii) a 3D printed cartridge enclosure, (iv) a mountable photocrosslinking system composed of a 3D printed case with an array of inexpensive 3 mm 405 nm LEDs (light emitting diodes), and (v) an array of external syringe pumps for hydraulic material extrusion. We demonstrated the versatility of this system by printing fibers with various shapes and material configurations, including different cross-sectional shaped fibers, grooved fibers, hollow fibers, multi-component fibers with material gradients along the fiber length or cross-section, co-axial, tri-axial and multiple-core fibers (figures 1(A) and (B)). Our platform also introduces a hydraulic-driven extrusion mechanism. This mechanism was chosen over current handheld extrusion mechanisms, such as pressure-driven extrusion [14] since the flow rate can be directly set on the syringe pump and remains constant regardless of the viscosity and temperature of the bioink, eliminating the need to adjust pressure values for different bioinks and temperature variations, which can be an arduous process, especially for low viscosity materials. Furthermore, having the syringe pumps separate from the device significantly reduces its size and weight compared to direct motor-driven extrusion mechanisms [15, 18], resulting in a more ergonomic and comfortable design for improved long-term operation while allowing for the addition of multiple materials and maintaining a compact form factor. This hydraulic approach also makes our device more accessible, as it is compatible with any commercial or 'DIY' syringe pump system. Furthermore, we also incorporated drug carriers, biochemical and biophysical cues to demonstrate the versatility of the handheld bioprinter in developing spatiotemporal drug delivery modules and wearable biosensors. Additionally, the proof of principle demonstration for the *in situ* printing of single-core and dual-core cell-laden fibers were illustrated to further extend the versatility of this platform in various biomedical applications.

2.2. Handheld printer for delivering multiple drugs

The bioprinted fiber can carry biologically active molecules such as drugs, growth factors and proteins for local delivery to the injury site to promote healing rate. We aimed to show that this system could be tailored to be used as a platform for the temporal and dosage-control delivery of different biomolecules (figure 2(A)). This feature allows us to precisely control over the release rate as well as deliver multiple agents during the healing period. This was achieved by printing fibers made of poly(ethylene glycol) diacrylate (PEGDA)-Laponite carrying different concentrations of poly(lactic-co-glycolic acid) (PLGA) particles (3, 6, 9 mg ml^{-1}), which were loaded with Rhodamine B (Rd) or 40 kDa fluorescein isothiocyanate-dextran (FITC-Dextran). The single-channel printhead was used to print both fiber types onto a petri dish, followed by photocrosslinking by illuminating 405 nm light at 20 mW cm^{-2} for 5 min.

As shown in figures 2(B) and (C), both profiles showed that the concentration of PLGA inside the fibers significantly impacts the dosage of released drug. These results indicated that the fiber with a PLGA concentration of 3 mg ml^{-1} released 246 ± 73 $\mu g\,ml^{-1}$ and 5 ± 1 ng ml^{-1} of FITC-Dextran and Rd, respectively, in five days, while these numbers increased to 6120 ± 125 ng ml^{-1} and 17 ± 2 ng ml^{-1} in the same time course for the fibers with 9 mg ml^{-1} PLGA concentration.

To demonstrate the capability of the handheld printer to produce fibers for on-demand drug release, we incorporated temperature-responsive Poly(N-isopropylacrylamide) (PNIPAM) microparticles in the printed fibers to trigger the release of biomolecules by an external stimulus (temperature).

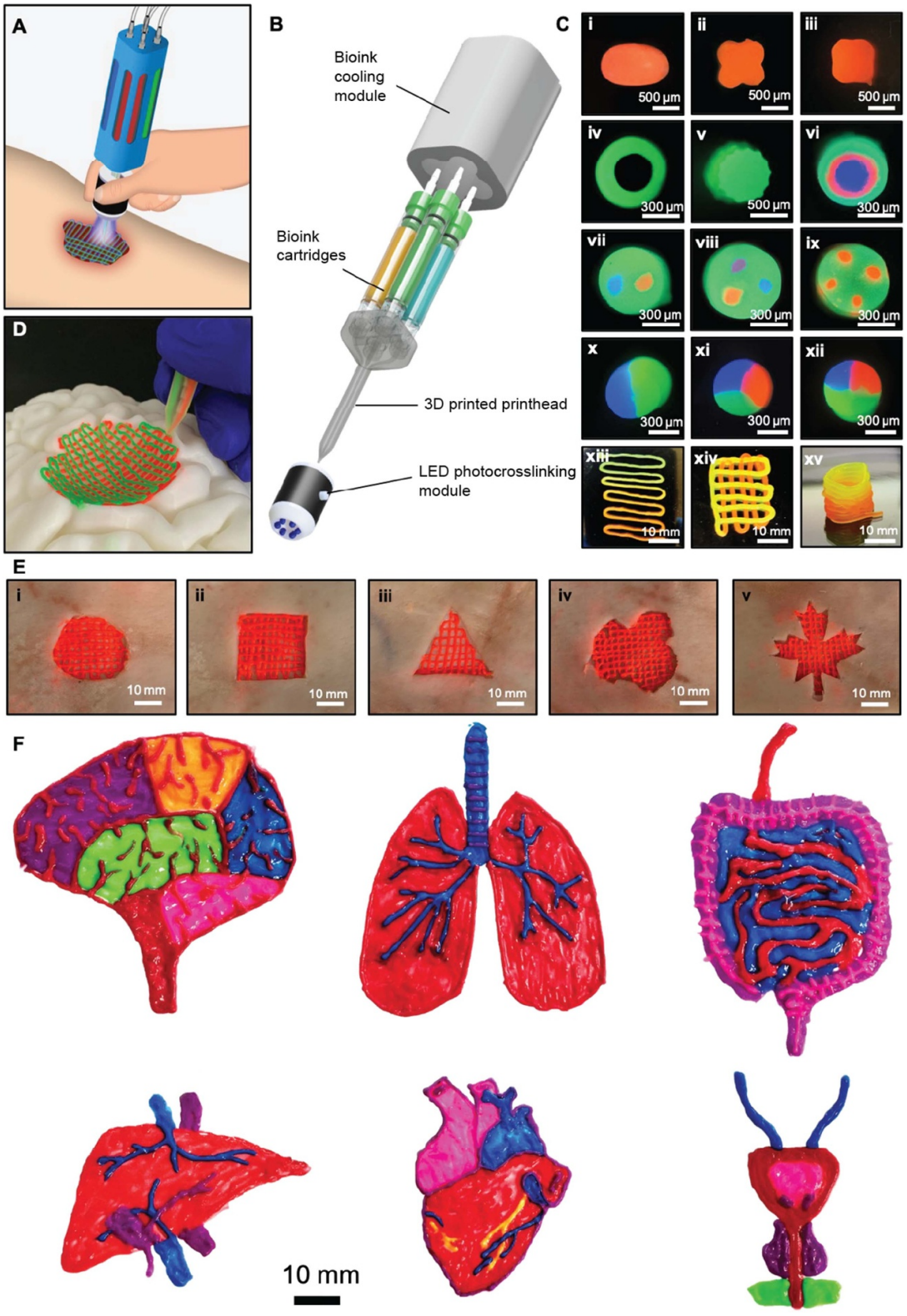

Figure 1. (A) Schematic of the design of the handheld bioprinter. (B) Schematic of the individual components of the device. (C) (i–xii) Cross-sectional views and (xiii–xv) photographic images of the different kinds of fibers produced with the different printhead configurations allowed by our platform. (D) Demonstration of handheld, *in situ* multi-material bioprinting on a curved surface. (E) Handheld bioprinted constructs produced on pig skins with various wound shapes. (F) Demonstrating the feasibility of producing complex constructs using multi-material printing.

To this end, we printed PEGDA-Laponite fibers loaded with PNIPAM microparticles. The PNIPAM microparticles were produced and loaded with FITC-Dextran according to our previously developed protocols [21]. As shown by figure 2(D), the FITC-Dextran release profile demonstrated a temperature-responsive behavior in which an increase in temperature from 20 to 42 °C resulted in significantly

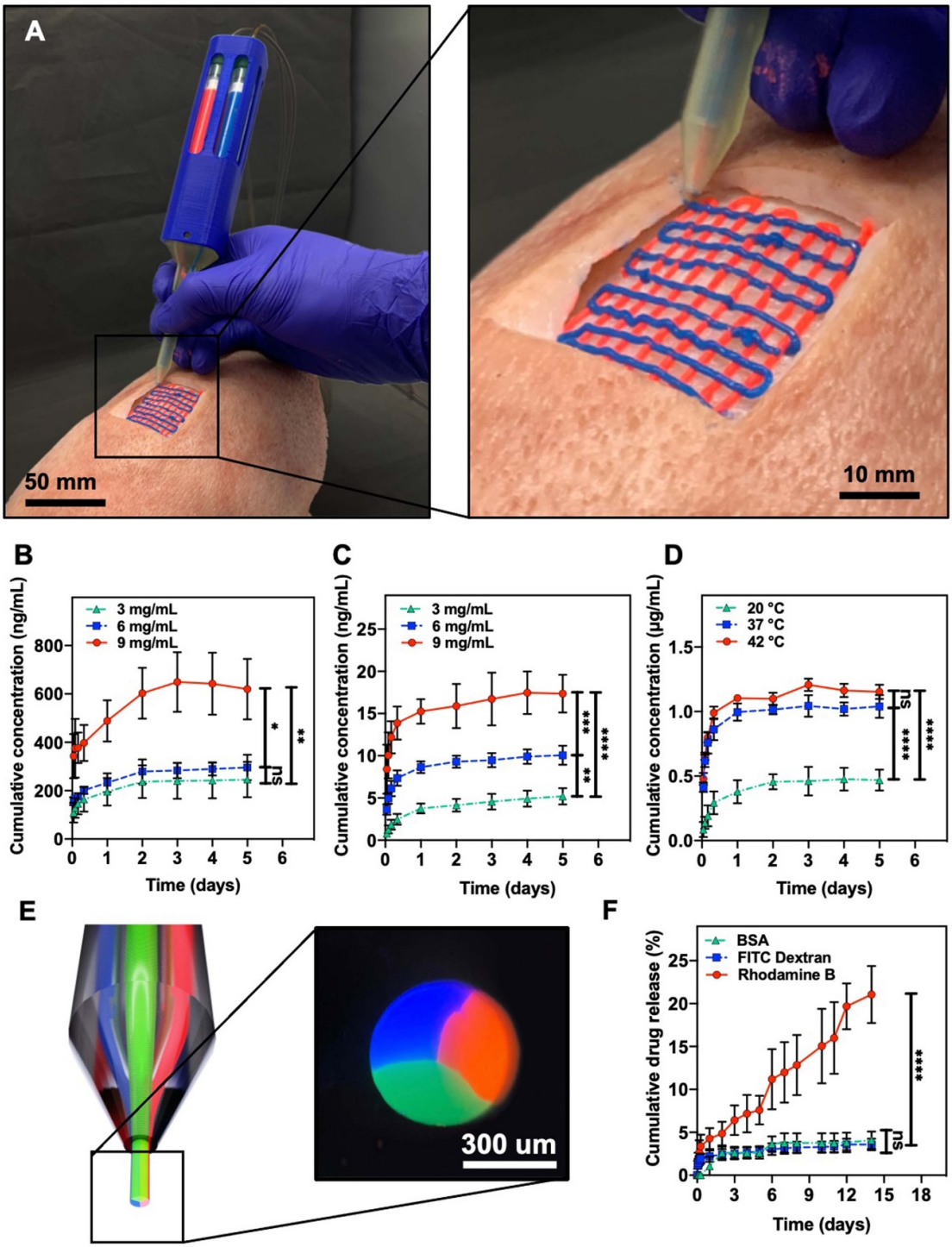

Figure 2. (A) Photographic image of handheld bioprinter printing a multi-material construct directly on an artificially made pig skin wound. Cumulative release of (B) FITC-loaded and (C) Rhodamine-loaded PLGA microparticles embedded in PEGDA-Laponite fibers with concentrations of 3, 6, and 9 mg ml^{-1} of microparticles in the fiber. (D) Cumulative release of FITC-loaded thermoresponsive PNIPAaM microparticles embedded in PEGDA-Laponite fibers, maintained at 20, 37, and 42 °C. (E) Schematic of tri-material printhead and microscopy image of the cross-section of the printed fiber. (F) Cumulative release of three-material fiber with BSA, FITC-Dextran and Rhodamine-loaded PLGA microparticles, embedded in each side of the fiber. The experiment was carried out with minimum of three replicates ($n = 3$). Results presented as mean ± SD ($^{*}p < 0.05$, $^{**}p < 0.01$, $^{***}p < 0.001$, and $^{****}p < 0.0001$).

higher diffusive flux of FITC-Dextran into the release medium. Later in this manuscript, we will show that electroconductive materials can be incorporated in the printed fibers, which can be used as an electronic system for facilitating heat-trigger drug release by altering the temperature. Equipping this temperature-responsive drug delivery composition with an electronic system allows for the activation

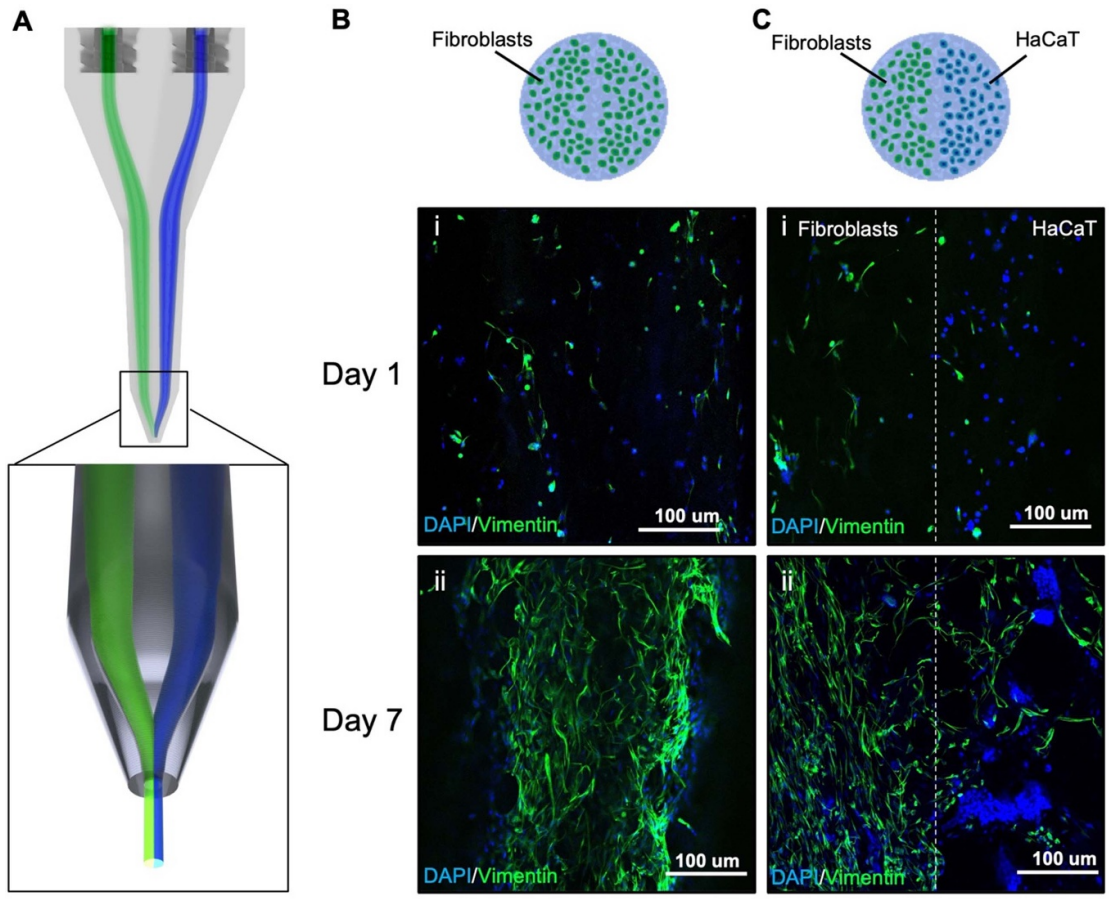

Figure 3. (A) Schematic images of the cross-sectional view and the tip of the dual-material printhead. Microscopy images of DAPI/Vimentin staining of (B) a monoculture of fibroblasts and (C) a co-culture of fibroblasts and HaCaT cells in each side of a GelMA-alginate fiber after (i) 1 and (ii) 7 d of culture.

of drug release from each individual fiber, providing precise control of the drug dosage by triggering an adequate quantity of drug-eluting fibers.

To demonstrate the ability to produce multi-compartment fibers loaded with different molecules in each compartment, we studied the release of a small drug model Rd, a growth factor model (FITC-Dextran) and a large protein model (bovine serum albumin (BSA)) from tri-material, side-by-side fibers over the time course of two weeks. All three molecules were loaded in PLGA microparticles and suspended in separate solutions of PEGDA 7.5% (w/v) to create three bioinks, each loaded with a different molecule. The three bioinks were fed onto each channel of the printhead (figure 2(E)), and printed onto a petri dish, photocrosslinking immediately upon deposition using the LED module.

The release profile of Rd-loaded PLGA carriers from the printed fiber showed a linear cumulative release to the level of 21.1 $\pm$ 3.2 (%) during the release period (figure 2(F)). The results indicated the size of the biomolecules had a significant impact on the release rate. The release rate of Rd reached significantly higher levels than BSA and FITC-Dextran, owing to the smaller size of Rd, which facilitates its flux from the pores presented in the PLGA microparticles and oriented fiber.

2.3. Multiple cells printing for co-culture studies

To demonstrate that our engineered handheld bioprinter has the capability to print multicell-laden fiber, we used a dual-material printhead that produced side-by-side materials in a single strand of a fiber (figure 3(A)). To this end, fibroblast and HaCaT cells were suspended each in a separate bioink composed of 1, 5, and 0.3% (w/v) alginate, GelMA, and lithium phenyl-2,4,6-trimethyl-benzoyl phosphinate (LAP), respectively. A mono-culture fiber configuration was made by feeding fibroblast-loaded bioink into both channels of the printhead. Separately, a co-culture fiber configuration was made by feeding fibroblast-loaded bioink through one channel, and HaCaT-loaded bioink through the other channel. Both channels merged into a single one before reaching the printhead's tip. The cell-laden fibers were wet spun into $CaCl_2$ 1% (w/v) in PBS solution, while simultaneously photocrosslinking with the LED module at 80 mW cm^{-2}. The encapsulated cells in the fibers were visualized and distinguished via staining nuclei with 4′,6-Diamidino-2-phenylindole

dihydrochloride (DAPI) and mesenchymal cells with vimentin (figures 3(B) and (C)). The confocal images showed that after 7 d of culture, both cell types populated across the fiber. Figure 3(B) shows that the fibroblast cells (stained positive with DAPI and Vimentin) completely covered the fiber after 7 d of culture in the mono-culture configuration. On the other hand, figure 3(C) shows that in the co-culture configuration, clusters of HaCaT cells (stained positive with DAPI) were formed in the right half of the fiber, while the fibroblast cells not only spread across the left half of fiber, but also partially infiltrated into the right half. Post-fabrication live/dead images of the produced fibers revealed that the majority of cells stained with calcein (live) implying that the fabrication technique had small effect on the cell viability (supplementary info—post-printing viability). Previously, Mirani *et al* [22] showed that UV crosslinking of cell-laden fibers can cause cell death and a reduction in the cell viability rate to less than 50%. Yet, our design's ultrafast, visible light photocrosslinking approach reduced the cell death caused by UV exposure.

2.4. Handheld printing of photocrosslinkable, cell-laden GelMA fibers

Photocrosslinkable polymers such as HAMA [23] and GelMA, [24] as well as polyethylene glycol derivates like PEGDA [25] hold great potential to be used in fabricating 3D cell-laden tissue models. It should be noted that the constructs made of photocrosslikable polymers have been shown to have high printing resolution [26]. Furthermore, the spatiotemporal control along with the low-temperature production mode offered by these photocrosslinkable bioinks facilitate 3D printing of complex cell-laden structures [27]. However, cell death caused by UV light irradiation and cytotoxicity induced by the photoinitiator (PI) is a challenge associated with 3D printing of cell-laden photocrosslinkable polymers. This fact highlights the importance of optimizing the dosage of PI and light parameters such as wavelength, intensity, and irradiation time to minimize these side effects [28]. Our system offers an ultrafast photocrosslinking approach using a low-cost LED sleeve (figures 4(A)–(D), movie 1). To demonstrate this feature, 3 million C2C12 cells were suspended in a 1 ml solution composed of 10% GelMA solution with 0.3% LAP and printed into rectilinear scaffolds. The nuclei and actin microfilaments of C2C12 cells encapsulated in the printed construct were visualized by DAPI/actin staining (figures 4(E) and (F)) and demonstrated cell spreading within bioink after 8 d of culture. The confocal image taken after one day showed an even 3D distribution of cell throughout the fiber (figure 4(G)). Notably, the results demonstrated that many of C2C12 cells developed a myotubule morphology by day 8. Post-printing cell viability was confirmed by an increase in the metabolic activity of cells encapsulated in bioprinted constructs up to two days (figure 4(H)). Taken together, these findings suggested that the printing technique did not cause any damage to the cells and that the cells were able to grow and proliferate once the printing process was completed.

To assess the suitability of these microfibers for cardiac tissue engineering, cardiomyocytes (CMs) isolated from neonatal mice were bioprinted using the handheld printer and the photocrosslinkable bioink. Cell functional properties were evaluated by immunofluorescence staining for DAPI/Actin/Troponin and beating properties of the constructs. The printed constructs showed a high level of Troponin T expression, demonstrating a high level of live CMs present within the fiber. CM-laden GelMA microfibers showed elongated and rod-shaped morphology of structural protein (F-actin) and contractile protein (Troponin-T), demonstrating relevant CM phenotype (figures 4(I) and (J), movie 2). The cells also exhibited beating after 5 d of culture (movie 3). Overall, our results indicated the feasibility of using the handheld bioprinter to create constructs for cardiac tissue engineering.

2.5. Coaxial bioprinting of cell-laden GelMA/alginate bioinks

Co-axial bioprinting has been widely used to create constructs from low-concentration bioinks [22]. The sheath flow often constitutes a crosslinking agent that rapidly cures the bioink while it leaves the printhead. The presence of the sheath flow also reduces the effect of wall shear forces being applied to cells, thus enhances post-printing cell viability [2]. The ability of our handheld bioprinter to create cell-laden constructs using co-axial flow printing is demonstrated by printing a composite bioink made of alignate and GelMA. The feasibility of this printing approach was demonstrated using two cell lines, including 3T3 fibroblasts and mouse CMs. We used $CaCl_2$ 1% (w/v) as the crosslinking agent through the sheath channel. Live/Dead assay was performed after 1 and 7 d, demonstrating high cell viability of more than 90% (figure 5(A-i)). Initially the cells were more rounded, but after 7 d, they showed a more elongated structure (figure 5(A-ii)). Separately, CMs were encapsulated in the bioink and printed in the same coaxial configuration. A live-dead assay also showed great cytocompatibility of the bioink after 7 d of culture (figure 5(B)).

2.6. Dual-core, multi-material fibers for tumor cell invasion

The handheld bioprinter was also used to produce hydrogel fibers with multiple cores, which enables creating multicellular structures. To showcase

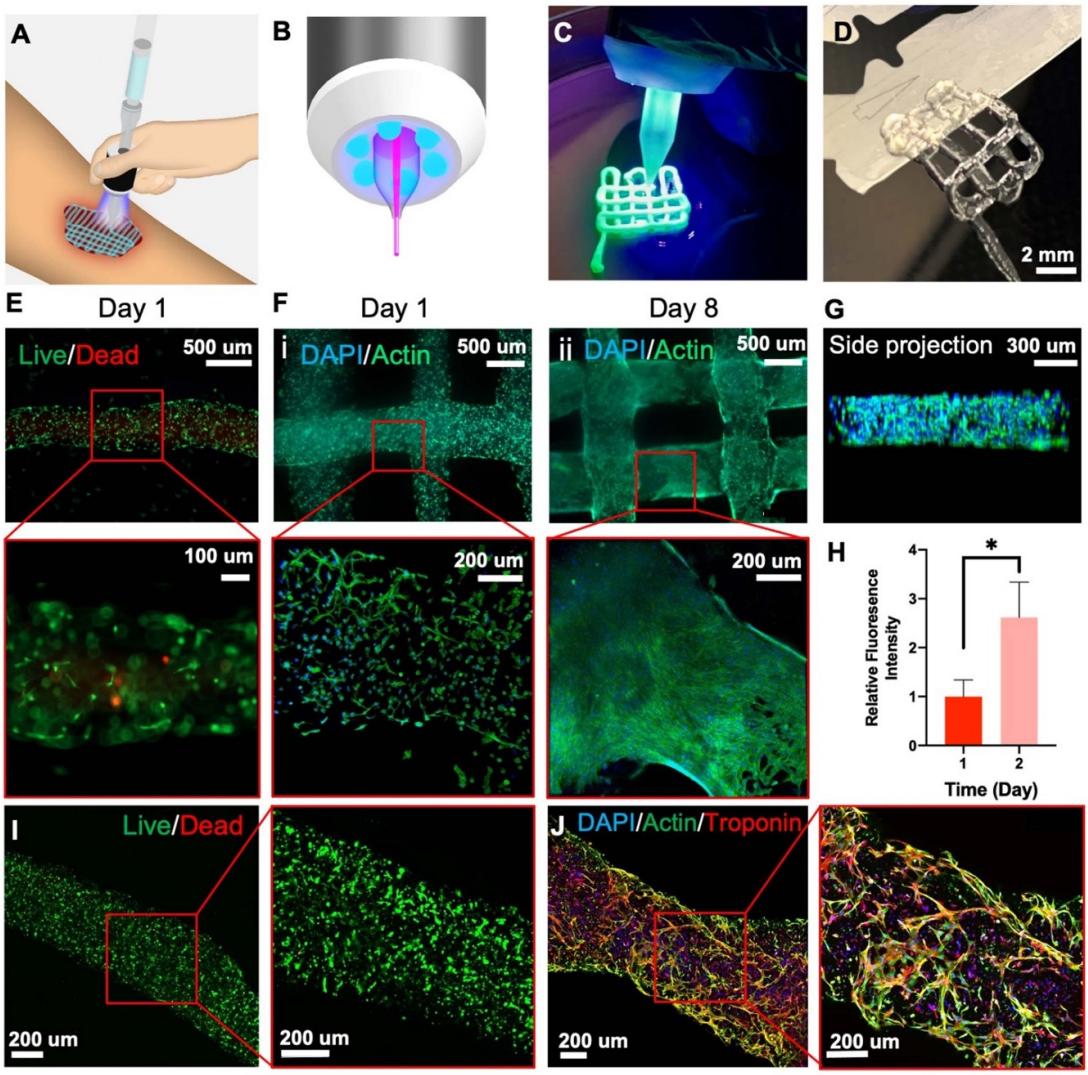

Figure 4. (A) Schematic image of the handheld bioprinter in its single-channel configuration with the mounted LED photocrosslinking module printing on a wound. (B) Schematic image of the tip of the printhead with the mounted LED module. (C) Photographic image of the device printing a two-layer, fluorescent dye-loaded GelMA mesh, immediately photocrosslinked upon printing by the LED module. (D) Photographic image of a printed and crosslinked cell-loaded GelMA mesh. (E) (i, ii) Live/Dead microscopy images of a C2C12-loaded GelMA fiber after 1 d of culturing. (F) DAPI/Actin microscopy images of the printed cell-loaded GelMA meshes after (i) 1 d and (ii) 8 d of culturing. (G) Side projection of the cell-loaded GelMA fiber. (H) Relative fluorescence intensity of the cell-loaded GelMA meshes after 1 and 2 d of culturing ($n = 3$, $^{*}p < 0.05$). (I) Live/dead assay of CMs encapsulated in GelMA bioink after 7 d of incubation. (J) DAPI/Actin/Troponin assay of CMs encapsulated in GelMA bioink after 5 d of incubation.

this capability, we produced constructs made of double-core fibers with GelMA 5% (w/v) in each core channel and a blend of GelMA 5% (w/v)/ alginate 1% (w/v) in the sheath channel. SKOV-3 cells were encapsulated into one of the core bioinks and human-derived fibroblast cells were encapsulated into the adjacent core to emulate a cancer-stroma microenvironment. The invasion profile of cells with and without fibroblasts was compared using a monoculture of SKOV-3 cells encapsulated in one core. The fluorescent images of the tumor and stromal cells inside the fibers revealed a time-dependent invasion pattern of the tumor cells into the matrix from the GelMA core of the fibers (figures 6(B) and (C)). This method enabled the production of meters of multicore fibers for analysis (figure 6(D)). Cell proliferation was indicated by metabolic activity measurement in both mono- and co-culture conditions, with co-culture systems demonstrating a higher rate of proliferation (figure 6(E)). The increased proliferation in the co-culture group was due to a greater number of cells, demonstrating that the printing technique had no effect on cell viability post-printing. After 3 d of culture, invasion length analysis revealed that SKOV-3 cells invaded longer when co-cultured with fibroblasts (figure 6(E)). This finding is in line with previous studies that demonstrated the role of cancer-associated fibroblasts on tumor growth and invasion

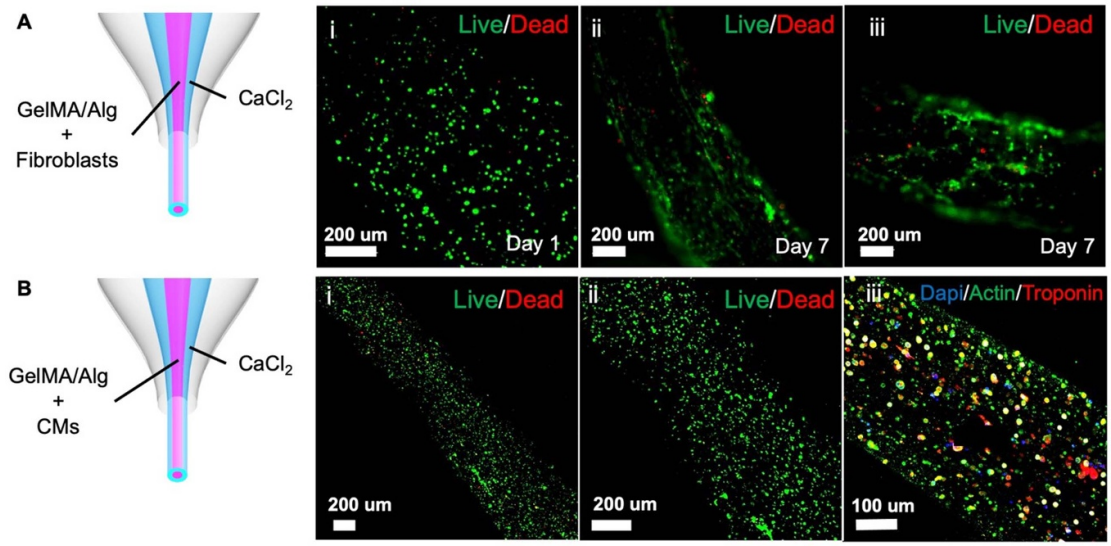

Figure 5. (A) Schematic image and Live/Dead assay of 3 T3 Fibroblasts encapsulated in GelMA/Alginate bioinks using coaxial printhead after (i) 1 and (ii, iii) 7 d of culture. (B) Schematic image, (i, ii) Live/Dead assay after 7 d of culture, and (iii) DAPI/Actin/Troponin assay after 5 d of culture of CMs encapsulated in GelMA/alginate bioinks using coaxial printhead.

[29]. Based on these findings, constructs made of multi-core fibers can be used an *in vitro* tool to model tumor microenvironment for drug screening applications.

2.7. Handheld printing of luminal constructs

Creating luminal constructs has major implications in tissue engineering and regenerative medicine. Creating highly vascularized tissues is central to the production of functional tissues with clinically relevant dimensions. Further, numerous tissues in the body are made of luminal structures that act as a physical and chemical barrier to ensure proper body function. Reproducing such structures requires a method that enables formation of hollow tubes that are perfusable [30]. To produce perfusable hollow fibers, we used a coaxial printhead to deposit core–shell fibers featuring a sacrificial core and a bioink shell (figure 7(A)). Our platform enabled the convenient manual deposition of perfusable fibers to generate constructs in various shapes and configurations (figures 7(B)–(G), movies 4–10) or three dimensions (figures 7(C) and (F)). Coaxial and dual-core printheads were used to demonstrate the feasibility of fabricating single-channel (figures 7(B)–(F)) or multichannel (figure 7(G)) hollow, perfusable vascular structures with consistent or varying diameters. To fabricate hollow fibers, an aqueous solution composed of alginate 2% (w/v) and Laponite 6% (w/v) bioink was flowed through the sheath channel while a solution of Poly(vinyl alcohol) (PVA) 10% (w/v) and $CaCl_2$ 1% (w/v) ran through the core channel(s) to induce ionic crosslinking of the alginate. Laponite was used in the alginate bioink to maintain structural integrity during fiber crosslinking. The outer and inner fiber diameters can be tuned by varying the core and sheath flow rates, as well as the printing speed (figure 7(D)).

2.8. Printing of biosensors

Implantable and wearable sensors hold great promise for continuous wound monitoring. The handheld bioprinter was used to demonstrate the ability to print sensors directly into the site of the injury. pH is one of the indicators of the skin's physiological condition and can serve as an effective real-time monitoring system. Previously we have developed color-changing pH sensor array for early detection of bacterial infections in wounds using image processing applications and smartphones [31]. In this approach, beads carrying a colorimetric pH-sensitive dye are incorporated in alginate 2% (w/v)/Laponite 6% (w/v). Figure 8(A) demonstrates the direct deposition of a pH-responsive colorimetric sensor on the generated artificial pig skin. As shown by the photographic image of the sensors exposed to buffers with different pH, the color of sensors changed from colorless to dark blue in response to variations in pH within the range of 7–8.75 (figure 8(B)). This method can be served as a point-of-care device to continuously monitor pH level of the defect area and examine the healing process. To extend the application of this platform, graphene oxide has been added to the starting alginate/Laponite bioink to induce electro conductivity to the printed fiber. This feature is widely applicable in developing biosensors, wearable or implantable bioelectronics, and heating element to trigger on-demand temperature-responsive drug release [32]. Furthermore, electroconductive hydrogels are versatile platforms for engineering neural and cardiac tissue [33]. This is because the stimulation of cellular behavior (i.e. differentiation, migration,

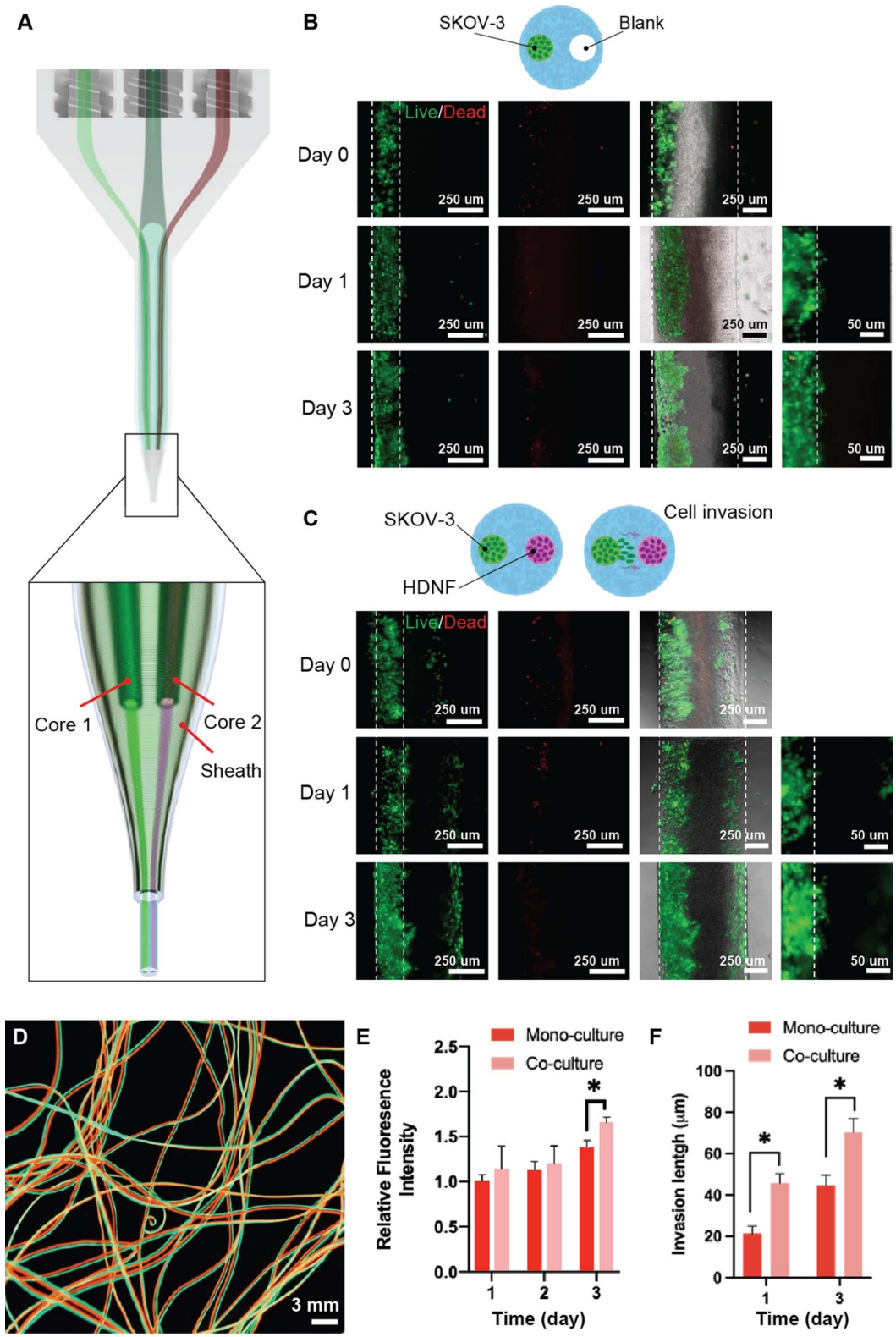

Figure 6. Schematic images of (A) the cross-sectional view and the tip of the dual-core printhead. Live/Dead fluorescent demonstration of invaded SKOV-3 cancer cells in dual-core GelMA/Alginate fibers from day 1 to day 3 in (B) monoculture of SKOV-3 cells, (C) Co-culture of SKOV-3/HNDF cells. (D) Photographic image of wetspun dual-core GelMA-alginate fibers, with each core loaded with either red or green fluorescent dye. (E) Relative fluorescence intensity shows the proliferation of SKOV-3 and SKOV-3/HNDF cells in mono-cultured and co-cultured GelMA-alginate fibers respectively. F) Invasion length of mono-cultured and co-cultured GelMA-alginate in dual-core fibers. Data are expressed as mean ± standard deviation ($n = 3$). * $p < 0.05$.

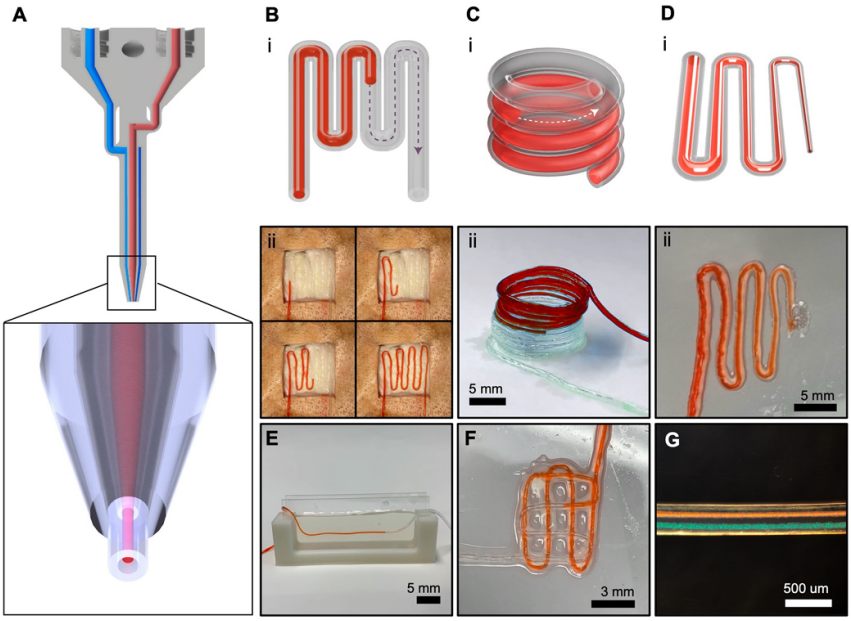

Figure 7. (A) Schematic images of the cross-sectional view and the tip of the coaxial printhead. (B-i), (C-i), (D-i) Schematic images with accompanying photographic images of (B-ii) a serpentine hollow, perfusable fiber printed directly on an artificially created pig skin wound, (C-ii) a spiral hollow, perfusable fiber and (D-ii) a hollow, perfusable fiber with varying diameter was made by varying printing speed. (E) Perfusable fiber embedded in a hydrogel matrix. (F) Multi-layer perfusable fiber. (G) Microscopy image a dual-channel hollow, perfusable fiber. All fibers were perfused with dye (red and/or green) for imaging.

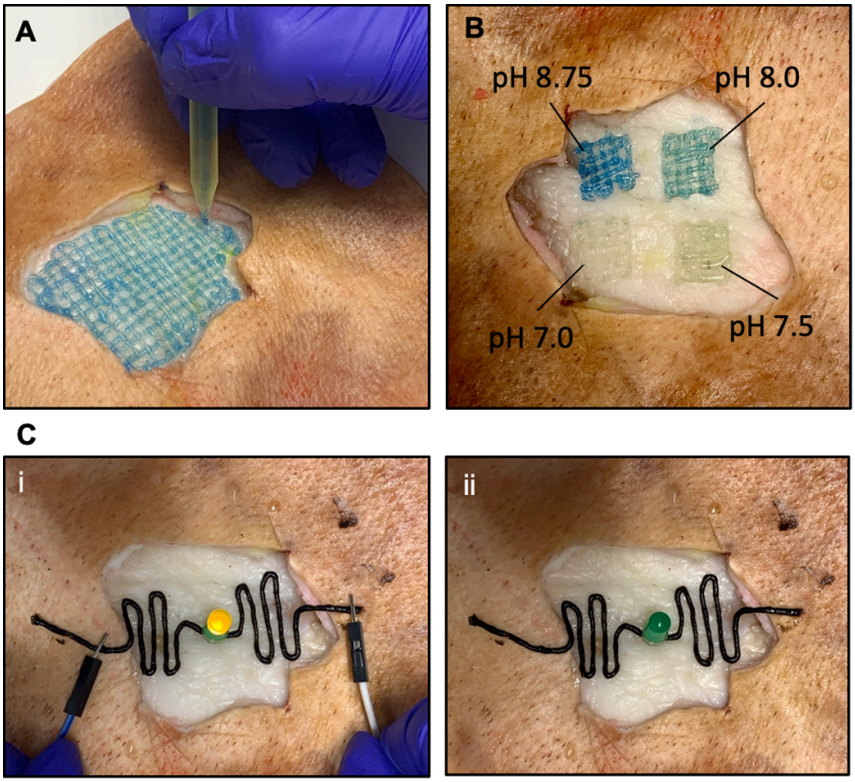

Figure 8. (A) Handheld bioprinting of pH-responsive colorimetric biosensors on an artificially generated pig skin wound. The biosensors allow for real-time detection of bacterial infection by changing color (B) from clear (healthy skin) to blue (infected skin). (C) (i-ii) Conductive hydrogel fibers bioprinted on an artificially generated pig skin wound illuminating an LED when voltage is applied to the fibers.

and proliferation) can be done by applying electrical, electrochemical, and electromechanical signals [33]. Figure 8(C)(i–ii) shows the capability of the handheld printer to produce electroconductive construct directly at a site of injury. As shown by the photographic image, two conductive fibers printed on the pig skin wound could illuminate a small LED when a voltage was applied from an external power supply.

3. Conclusion

In this research we presented a novel, low-cost handheld bioprinting platform, that enables *in situ* deposition of functional hydrogel fibers and different types of cells such as dermal fibroblasts, HaCaT, C2C12, and SKOV-3 cells. The printheads were fabricated with a high-resolution SLA-DLP 3D printer. The platform's modularity allows for the equipment of a mountable low-cost photocrosslinking system and conventional pneumatic Luer lock cartridges, as well as facilitating easy and rapid modification of the device for different bioink compositions and printing geometries. Overall, our platform enables the direct extrusion of fibers with different morphological characteristics, size, cross-sections, and material gradients at the injury site. Additionally, our handheld bioprinter can print fibers with a wide range of materials such as alginate, GelMA, and PEGDA in pure or hybrid forms using different crosslinking approaches. The printed fibers have the versatility to be augmented with drug carriers, conductive materials, and pH-responsive sensors, which extend the application of the printed fibers to the developing spatial and temporal local drug delivery systems, tissue engineering scaffolds, and wearable biosensors and bioelectronics. Furthermore, having multichannel cartridge design allows printing multicore cell-laden fibers in which different types of cells are co-cultured and proliferated, showing the feasibility of our handheld bioprinter for the direct cell delivery applications. This ability to produce dual core cell laden hydrogel fiber provides the opportunity to study the biological behavior of cancer cells *in vitro*. Taking everything into consideration, in the context of regenerative medicine, this convenient technology is attractive for clinical settings for the efficient delivery of cells and therapeutic agents.

4. Materials and methods

4.1. Chemicals

Polylactic acid (PLA), Gelatin Type A from porcine skin, Methacrylic anhydride (MA), LAP, alginate, Poly(ethylene glycol) diacrylate (PEGDA, $Mn = 2000$ Da), graphene oxide, PVA, Hank's balanced salt solution, Rhodamine B (Rd), BSA, 20 KDa FITC-Dextran, dichloromethane (DCM), PLGA, PNIPAM, N,N′-methylenebis (acrylamide) (BIS), 2-hydroxy-4′-(2-hydroxyethoxy)-2-methylpropiophenone as PI, ammonium persulfate (APS), Span 80, α-naphtholphthalein, Dowex 1 × 4 chloride form beads, Triton-X100, DAPI and PBS tablets were purchased from Sigma-Aldrich (Burlington, USA). The rest of suppliers were indicated in the text.

4.2. Handheld bioprinter design

The 3 ml bioink cartridges were purchased from Cellink (BICO, Gothenburg, Sweden). To fit within the compact design of the device, the barrel flanges were cut with an Exacto knife and replaced with the 3D-printed barbed connectors. Individual syringe pumps (Harvard Apparatus, Holliston, USA) with water-loaded syringes were connected to the barbed ends of the cartridges with plastic tubing for hydraulic actuation-powered extrusion. The bioink cartridges were attached to the printhead with female-to-female Luer lock connectors. Six 3 mm 405 nm LEDs (Mouser Electronics, Mansfield, USA) and a push-button were embedded in the 3D-printed light curing case and connected in series, powered by two 9 V batteries to supply 3 V to each LED. All custom components of the handheld bioprinter were designed using Fusion 360 software (Autodesk, Inc., San Francisco, USA). The housing and LED case were printed in PLA material on an Ultimaker 2 3D printer (Ultimaker, Utrecht, Netherlands). The printheads and barbed attachments were printed in photocurable resin using a Kudo3D Micro SLA 3D printer (Kudo3D, Dublin, USA).

4.3. Bioink preparations

4.3.1. Sterile GelMA

Lyophilized GelMA was prepared using the method described in our previous work [22]. Briefly, type-A gelatin from porcine skin was dissolved in PBS at a concentration of 5% (w/v) at 60 °C. MA was slowly added to the gelatin solution while stirring at 300 rpm. The solution was stirred for 3 h and transferred into 12–14 kDa dialysis membranes. The membranes were placed in a large beaker with deionized water at 50 °C. The water was replaced twice a day for 7 d to remove unreacted MA. The solution was then filtered and lyophilized for 3 d to obtain solid GelMA. GelMA bioink was made by dissolving solid GelMA in Dulbecco's Modified Eagle's Medium (DMEM) (Thermo Fisher Scientific, Waltham, USA. Cat# 11 965 084) mixed with LAP. GelMA and LAP concentrations varied for different tests. The final solution was filtered with a 0.2 μm sterile filter.

4.3.2. Alginate-Laponite

An alginate stock solution was made by dissolving sodium alginate powder in deionized (DI) water at a concentration of 4% (w/v) and kept at 60 °C for 1 h while stirring. The solution was then transferred

into a syringe. Separately, Laponite stock solution was made by adding Laponite powder (BYK, Wesel, Germany) to a falcon tube with DI water at a concentration of 12% (w/v) at 4 °C to prevent immediate gelation and vortexed for 2 min. The contents were immediately transferred into a syringe for the solution to gelate without creating bubbles. Both alginate and Laponite stock solutions were mixed at a 50:50 ratio by connecting both syringes with a female-to-female Luer lock adapter and repeatedly pushing the material back and forth between both syringes, resulting in a homogeneous solution with final concentrations of 2% (w/v) alginate and 6% (w/v) Laponite.

4.3.3. PEGDA

PEGDA bioink was made by dissolving LAP in distilled water at 60 °C at a concentration of 0.3% (w/v). The solution was left in a water bath at 60 °C for 15 min, periodically vortexing every 5 min. PEGDA was then added to the solution to a concentration of 7.5% (v/v) and vortexed for 2 min. The solution was then transferred into a syringe.

4.3.4. PEGDA-Laponite

A PEGDA stock solution was made by dissolving LAP in distilled water at 60 °C at a concentration of 0.6% (w/v). The solution was left in a water bath at 60 °C for 15 min, periodically vortexing every 5 min. PEGDA was then added to the solution to a concentration of 15% (v/v) and vortexed for 2 min. The solution was then transferred into a syringe. Separately, a 12% (w/v) Laponite stock solution was prepared using the same method described in the 'alginate/Laponite' bioink section above. Both PEGDA and Laponite stock solutions were mixed at a 50:50 ratio by connecting both syringes with a female-to-female Luer lock adapter and repeatedly pushing the material back and forth between both syringes, resulting in a homogeneous solution with final concentrations of 6% (v/v) PEGDA, 0.3% (w/v) LAP and 6% (w/v) Laponite.

4.3.5. Sterile alginate-GelMA

Alginate powder was sterilized by suspending it in anhydrous ethanol in a 15 ml Falcon tube and left without a lid inside a biosafety cabinet (BSC) until the ethanol was fully evaporated. An alginate stock solution was prepared by dissolving the sterilized powder in DMEM at 2% (w/v). A separate stock solution of 10% (w/v) GelMA and 0.6% (w/v) LAP was prepared in DMEM and filtered with a 0.2 μm acetate cellulose syringe filter. Both GelMA and alginate stock solutions were mixed at a 50:50 ratio by connecting both syringes with a female-to-female Luer lock adapter and repeatedly pushing the material back and forth between both syringes, resulting in a homogeneous solution with final concentrations of 5% (w/v) GelMA, 0.3% (w/v) LAP and 1% (w/v) alginate.

4.3.6. pH-responsive ink

pH-responsive bioink was prepared using the method described in our previous work [4] with slight modifications. Briefly, about 135 mg of α-naphtholphthalein dye was dissolved in a beaker with 6 ml of 100% ethanol, followed by the addition of 24 ml dH2O and stirred for 30 min. 3300 mg of Dowex 1 $\times$ 4 chloride form beads were washed in a 50 ml Falcon tube with DI water by vortexing for 2 min, letting the beads fully sediment and replacing the supernatant. This washing step was repeated twice with DI water and once with 100% ethanol. After removing the ethanol, 30 ml of DI water was added to the beads, the suspension was vortexed for 2 min and added to the α-naphtholphthalein dye solution. The final suspension was washed multiple times by vortexing, waiting for the beads to sediment and replacing the supernatant with DI water until the supernatant was completely transparent. Sodium alginate powder was then added to the bead suspension to reach a concentration of 2% (w/v) and stirred until fully dissolved. The contents were cooled down to 4 °C. Laponite powder was then added at a concentration of 6% (w/v) and vortexed for 1 min. The contents were immediately transferred to a syringe before gelation of the Laponite to prevent bubbles.

4.3.7. Conductive ink

Graphene oxide bioink was prepared using the method described in our previous work [34] with slight modifications. Briefly, graphene oxide was added to DI water at a concentration of 5 mg ml^{-1} and sonicated for 5 min. Alginate powder was added to the suspension at a concentration of 0.5% (w/v) and vortexed for 5 min. The solution was cooled to 4 °C. Laponite powder was then added at a concentration of 6% (w/v) and vortexed for 2 min. The contents were immediately transferred into a syringe for the solution to gelate without creating bubbles.

4.3.8. Cell-laden bioinks

The desired cells were dissociated and centrifuged to prepare the cell-laden bioink, and the entire supernatant was carefully removed. Using a pipette with the tip cut, the desired sterile bioink was added to the cell pellet which was resuspended by gentle pipetting.

4.3.9. PVA-$CaCl_2$ sacrificial crosslinking solution

PVA powder was added to distilled water at a concentration of 10% (w/v) and stirred at 60 °C until fully dissolved. $CaCl_2$ powder (Fisher Scientific, Pittsburgh, USA) was then added to the solution at a concentration of 1% (w/v) and vortexed for 2 min.

4.3.10. Preparation of drug-eluting PLGA microparticles

The drug models were initially loaded on the PLGA microparticles. The double (W1/O/W2) emulsion/

solvent evaporation technique was used to prepare drug-loaded PLGA microparticles. In brief, 1 ml PVA 1% (w/v) aqueous solution containing 1 mg of the drug (Rd, FITC-Dextran or BSA) (W1) was emulsified into 5 ml of DCM solution containing 10% (w/v) PLGA and vortexed for 1 min to prepare the primary W1/O emulsion. After that, 20 ml of 0.5% (w/v) PVA solution (W2) was added to the primary W1/O emulsion and vortexed for 1 min. The prepared W1/O/W2 emulsion was then added to 80 ml of 0.2% (w/v) PVA solution and stirred for 4 h at 35 °C to allow the organic solvent to evaporate. To obtain the drug-loaded PLGA microparticles, the emulsion was centrifuged at 350 × g for 5 min. Finally, the obtained microparticles were washed three times in distilled water and freeze-dried.

4.3.11. Preparation of thermoresponsive, drug-eluting PNIPAM microparticles

PNIPAM microparticles prepared according to the previously published method with the assist of microfluidic flow-focusing droplet generators [21]. Briefly, the dispersed solution was prepared by dissolving PNIPAM (10%, w/v), BIS 0.4% (w/v), PI 1% (w/v), and APS 0.6% (w/v) in distilled water. The dispersed phase and continuous phase composed of mineral oil and span 80 10% (v/v) were injected into a microfluidic chip using 1 ml and 10 ml syringes connected to the chip's inlets with Tygon tubings. These syringes were mounted on syringe pumps (Harvard Apparatus Holliston, USA) to precisely control the flow rates of continuous and dispersed phases. *In situ* photopolymerization of the microparticles was carried out when the generated microcarriers passed through a coil-shaped collecting tube while being exposed to UV light (20 mW cm^{-2}) for 15 min. To separate microparticles from oil, they were centrifuged and washed two times with soap solution (1% v/v in distilled water) followed by four times rinse in distilled water. Finally, the collected microparticles were lyophilized and then stored at 5 °C.

FITC-Dextran was passively loaded onto the microparticles by immersing 10 mg of the lyophilized particles into a 1 ml of FITC-Dextran solution (1 mg ml^{-1}) for 48 h. The suspension vortexed every 12 h to ensure that FITC-Dextran was uniformly loaded on the carriers. Then, the suspension was centrifuged to remove the FITC-dextran solution followed by washing the particles three times with cold water (15 °C).

4.3.12. Bioprinting process

For all bioink/printhead configurations, the extrusion rate of each channel was individually adjusted by setting the flow rate of their respective syringe pumps to the desired value. Bioprinting started as soon as all the materials reached the tip of the printhead. The printing surface or wet spinning media varied for each test. It should be noted that for all cell work, the interiors of the printhead, hydrogel cartridges, connectors, and tubing were all sterilized with 70% ethanol and washed twice with PBS before printing the cells. Also, the exterior of all components were sprayed with 70% ethanol. The tubing and each cartridge were then filled with PBS and a syringe with PBS was connected to a syringe pump for hydraulic actuation of each cartridge.

4.3.13. Preparation and perfusion of hollow, vascular fibers

Alginate–Laponite bioink was loaded into one cartridge and attached to the sheath channel of the coaxial printhead. PVA-$CaCl_2$ sacrificial crosslinking solution was loaded into a separate cartridge and attached to the core channel of the printhead. For dual-core fibers, two cartridges with PVA-$CaCl_2$ were attached to each core channel of the dual-core printhead. The fibers were printed on a petri dish or an artificially made pig skin wound. $CaCl_2$ 1% (w/v) was deposited over the fibers immediately after printing to accelerate crosslinking. The sacrificial PVA-$CaCl_2$ solution was cleared from the internal fiber channel using an air-filled syringe with a 25 G needle inserted at the end of the fiber. The fiber was then perfused with dye using the same syringe and needle.

4.3.14. Preparation and release study of single-channel, drug-eluting fibers

For single-channel drug-eluting fibers, drug-loaded PLGA microparticles were dispersed into PEGDA-Laponite bioink at concentrations of 3, 6, and 9 mg ml^{-1}. Each drug-eluting fiber was made by extruding 60 μl of the PLGA-loaded bioink followed by photopolymerizing for 5 min under 405 nm visible light.

To measure the drug release rate of FITC-dextran and Rh, the fiber loaded with PLGA drug carriers was immersed in 300 μl of PBS and incubated at 37 °C. At predefined timepoints (1, 2, 4, 8, 24, 48, 72, 96, and 120 h), 100 μl of the release medium sample was collected to measure the drug concentration and replaced with 100 μl of fresh PBS. The fluorescence intensity of the collected medium at each time point was measured using a Tecan Infinite M Nano plate reader at λ_{ex} 490 nm λem^{-1} 520 nm for FITC dextran, and λ_{ex} 546 nm λem^{-1} 585 nm for Rh. Using the relevant calibration curve, the acquired fluorescence intensity was converted to concentration (mg ml^{-1}). To avoid dilution error, calculation of released concentration of drug was carried out as follows:

$$C_n = C_{n-1} + \Delta C$$

$$\Delta C = C'_n - C'_{n-1}$$

where C_n and C_{n-1} are the cumulative concentrations of drug at the nth and $(n-1)^{th}$ time points, C'_n

represents the measured concentration of drug at the n^{th} time point, and C'_{n-1} indicates the diluted concentration of drug at the $(n-1)^{th}$ timepoint.

4.3.15. Preparation and release study of three-channel, drug-eluting fibers

PLGA microparticles loaded with BSA, FITC-Dextran and Rh were dispersed into three separate PEGDA bioinks at a concentration of 18 mg ml^{-1} (PLGA/bioink). All three bioinks were loaded into three separate cartridges. The cartridges were attached to each channel of the tri-material printhead with the LED module attached. The tri-drug-eluting fibers were made by extruding all bioinks at the same flow rate until a total of 60 μl was extruded. The resulting fiber had a concentration of 6 mg ml^{-1} of each drug-loaded microparticles.

To measure the release of three drugs (FITC dextran, Rh, and BSA) from the fiber, 60 μl of drug-loaded fiber was incubated in 300 μl of PBS. To maintain a constant volume of release medium, 100 μl of the medium sample was obtained to test the drug concentration at predefined time intervals (1, 2, 4, 8, 24, 48, 72, 96, 120, 144, 168, 192, 240, 268, 292, and 336 h), and 100 μl of fresh PBS was supplied. The fluorescence intensity of the withdrawn medium at each time point was measured using a Tecan Infinite M Nano plate reader to determine the release of FITC dextran and Rh (λ_{ex} 490 nm λem^{-1} 520 nm for FITC dextran, and λ_{ex} 546 nm λem^{-1} 585 nm for Rh). Using the relevant calibration curve, the acquired fluorescence intensity was converted to concentration (mg ml^{-1}). For the BSA, 500 μl of Bradford Reagent was added to 10 μl of the sample. The absorbance of predetermined concentrations were measured at 595 nm using the plate reader to generate a standard curve which was later used to calculate the unknown concentrations of BSA released from printed meshes. Finally, based on the cumulative concentrations obtained as described before, the drug release percentage at various time periods was calculated. Six replicates were used in each drug release experiment.

4.3.16. Preparation and release study of thermo-responsive drug-eluting fibers

Thermoresponsive, drug-eluting PNIPAM microparticles were dispersed into PEGDA-Laponite bioink at a concentration of 10 mg ml^{-1}. Each drug-eluting fiber was made by extruding 60 μl of the blended ink followed by photopolymerizing for 5 min under 405 nm visible light. After that, the release experiment was carried out by immersing the prepared fibers in 300 μl of PBS at 20, 37, 42 °C in pH 7.4. At predefined time intervals (1, 2, 4, 8, 24, 48, 72, 96, and 120 h), 100 μl of the supernatant was taken for analysis and replaced with fresh PBS with temperature similar to that of release condition. The concentration of FITC-Dextran in the supernatant was analyzed by measuring the fluorescence intensity at an excitation peak of 490 nm and an emission peak of 520 nm using a plate reader (Tecan Infinite M200Pro). The cumulative FITC-Dextran release from fibers was calculated via converting fluorescence intensity to concentration by the prepared standard calibration curve and obtaining the cumulative concentrations according to the previously mentioned method. This experiment was performed in triplicates.

4.3.17. Statistical analysis

A minimum of three repetitions were used in each experiment, and the data were presented as mean ± standard deviation (SD). Using GraphPad Prism 7.0, a one-way ANOVA with Tukey's multiple comparisons was performed to compare the means. The following values were noted for statistical significance: $^{*}p < 0.05$, $^{**}p < 0.01$, $^{***}p < 0.001$, and $^{****}p < 0.0001$.

4.3.18. Preparation of pH-responsive, colorimetric meshes

pH-responsive colorimetric bioink was loaded into a cartridge and attached to the single-channel printhead. Two-layer meshes were printed directly on an artificially made pig skin wound, and crosslinked by adding 1 ml of $CaCl_2$ 1% (w/v) solution to each fiber and let sit for 3 min. The excess $CaCl_2$ was removed with a Kimwipe. 200 μl of buffer solutions at different pH values (7, 7.5, 8, 8.75) were added to each mesh and let sit for 1 h for colorimetric response to take effect.

4.3.19. Preparation of conductive, graphene oxide fibers

Graphene oxide bioink was loaded into a cartridge and attached to the single-channel printhead. Two fibers were printed directly on an artificially made pig skin wound and crosslinked by adding 1 ml of $CaCl_2$ 1% (w/v) solution to each fiber and let sit for 3 min. The excess $CaCl_2$ was removed with a Kimwipe and the fibers and underlying pig skin were washed twice with DI water.

4.3.20. Preparation of dual-material cell-laden fibers

Two separate sterile alginate-GelMA bioink solutions were loaded with HaCaT cells and fibroblasts, respectively. Two cartridges were loaded with the fibroblast-laden bioink, and one cartridge was loaded with HaCaT cell-laden bioink. For mono-culture configuration, the two fibroblast-laden cartridges were attached to either side of the dual-material printhead. For co-culture configuration, one fibroblast-laden cartridge was attached to one channel and the HaCaT cell-laden cartridge was attached to the other. Both configurations were wet spun by inserting the tip of the printhead into a bath of Hank's balanced

salt solution (HBSS) containing 1% $CaCl_2$, while simultaneously photocrosslinking with the LED module at 80 mW cm^{-2}.

4.3.21. Preparation of photocrosslinkable cell-laden GelMA fibers

Sterile GelMA 10% (w/v) + LAP 0.3% (w/v) bioink solution was loaded with C2C12 myoblasts cells (ATCC CRL-1772) (3×10^6 cell ml^{-1}) or CMs (15×10^6 cell ml^{-1}). The cartridge was cooled down to 15 °C For thermal gelation of GelMA prior to printing. The LED module and cooling sleeve (stored at 4 °C) were mounted to the printhead. Fibers or meshes were printed on a petri dish inside the BSC while simultaneously being photocrosslinked with the LED module. The constructs were then transferred to culture media.

4.3.22. Preparation of dual-core cell-laden fibers for modeling tumor invasion

The *in vitro* tumor model was made the wet spinning of dual-core fibers including two compartments for tumor and stroma. Alginate/GelMA bioink was loaded into one cartridge and attached to the sheath channel of the dual-core printhead. Three separate sterile GelMA 5% (w/v) + LAP 0.3% (w/v) solutions were loaded with either fibroblast cells (2×10^6 cell ml^{-1}), human ovarian cancer cell line (SKOV-3) (4×10^6 cell ml^{-1}), or left without cells (blank). All three solutions were loaded into three separate cartridges. To recapitulate the tumor microenvironment *in vitro* including the crosstalk of the stromal cells and tumor cells and its role in the invasive behavior of the tumor cells, two experimental conditions were designed. For the mono-culture configuration, the cartridges with SKOV-3 cells and fibroblasts were attached to the core channels of the printhead, whereas for the co-culture configuration, the cartridges with SKOV-3 cells and blank were attached to the core channels. Both configurations were wet spun by inserting the tip of the printhead into a bath of HBSS containing 1% $CaCl_2$, while simultaneously being photocrosslinked with the LED module attached to the printhead. Afterwards, they were removed from the bath and incubated in the culture media for up to 72 h.

4.3.23. Cell culture

Human neonatal dermal fibroblasts (ATCC PCS-201-010) were cultured in high glucose DMEM supplemented with 10% fetal bovine serum (FBS) (Thermo Fisher Scientific, Waltham, USA. Cat# 10437028) and 1% (v/v) penicillin-streptomycin (Pen Strep) (Thermo Fisher Scientific, Waltham, USA. Cat# 15140122) in an atmosphere of 5% CO2 at 37 °C. Cells were cultured in a Corning T-75 cm^2 Rectangular Canted Neck Cell Culture Flask and passaged with TrypLE Express (Thermo Fisher Scientific, Waltham, USA. Cat# 12605093) once they got around 90% confluence. HaCaT cells (AddexBio, San Diego, USA. Cat# T0020001), a transformed human keratinocyte cell line, were cultured in high glucose DMEM with 10% FBS in Corning T-75 cm^2 Rectangular Canted Neck Cell Culture Flask and passaged with Trypsin-EDTA (Thermo Fisher Scientific, Waltham, USA. Cat# 25200072). The culturing protocol for C2C12 myoblasts cells (ATCC CRL-1772) and human ovarian cancer cell line SKOV-3 cells (ATCC HTB-77) was the same as the protocol for HaCaT cells.

NIH-3T3 (ATCC CRL-1658) fibroblasts were cultured in a medium composed of DMEM supplemented with 10% FBS and 1% antibiotic in a sterile incubator (Heracell Vios 160i, Thermo Fisher Scientific, Waltham, USA) with 5% CO_2 at 37 °C. The cells were passaged after reaching around 80% confluence.

4.3.24. Neonatal rat CM isolation

Neonatal Sprague-Dawley rats (2d old) were obtained from Charles River Laboratories (Wilmington, USA) and were euthanized based on the protocol approved by the Animal Ethics Committee of the Centre Hospitalier Universitaire Sainte-Justine Research Centre (CRCHUSJ, protocol number: 2021–3018). All the procedures were in accordance with the guidelines of the Canadian Council on Animal Care and the US National Institutes of Health Guide for the Care and Use of Laboratory Animals. Briefly, the hearts were collected into HBSS cold buffer, cut into smaller sections, washed with cold HBSS two times, and digested into single cardiac cells by the Neonatal Heart Dissociation Kit (Miltenyi Biotec, Bergisch Gladbach, Germany) based on the recommended protocol of the manufacturer. After digestion, cells were pre-plated in DMEM-F12 (supplemented with 10% FBS, 1% Pen Strep, 0.2% BSA, Insulin-Transferrin-Selenium solution [1:200], and 0.1 mM ascorbic acid) for 1 h. Finally, CMs were isolated from cardiac fibroblasts via centrifugation as a cell pellet.

4.3.25. Cell viability assessment

Printed samples were transferred to the six well-plate and cultured containing the specific cell growth media in an atmosphere of 5% CO2 at 37 °C. To determine the cell viability, a live/dead cell viability kit (Invitrogen, Waltham, USA, Cat# L3224) was used following the manufacturer's instructions. The fibroblast, HaCaT, and SKOV-3 cell-laden fibers or meshes were incubated in the live/dead solution for 30 min while protected from light at room temperature. The hydrogels were then washed once with PBS and imaged with a Zeiss Axio Observer 5 fluorescent microscope (Zeiss, Germany). For CM-laden fibers, the fibers were washed with HBSS three times and were further imaged by either Leica DMi8 wide-field

or SP8-DLS confocal microscopes (Leica Biosystems, Germany).

4.3.26. Immunofluorescence and actin staining
For fibroblast, HaCaT and C2C12 cell-laden fibers: fibers were fixed with 10% neutral buffered formalin (Thermo Fisher Scientific, Waltham, USA, Cat# 22-220682) for 45 min at room temperature and then washed three times with PBS. The fibers were permeabilized with 0.3% Triton-X100 in PBS for 10 min, then incubated in a blocking buffer of 3% BSA and 0.3% Triton-X100 in PBS for 30 min. The primary antibody solutions were prepared in 1% BSA and 0.3% Triton-X100 in PBS with a dilution of 1:200 for anti-vimentin conjugated to AlexaFluor 488 (Thermo Fisher Scientific, Waltham, USA, Cat# Z25402). Actin staining solutions (Thermo Fisher Scientific, Waltham, USA, Cat# A12379) were prepared by dilution in PBS as per the manufacturers protocol. For antibody staining, hydrogel fibers were incubated in the primary antibody solution overnight at 4 °C protected from light. For actin staining, the fibers were instead incubated in actin staining solution for 2 h at room temperature. All fibers were then washed three times with PBS and the nuclei were counterstained with 5 μg ml^{-1} DAPI for 10 min. The fibers were again washed three times with PBS and finally imaged with a Zeiss Axio Observer 5 fluorescent microscope.

For CM-laden fibers: After 5 d of culture, CM-laden fibers were fixed into 3.7% (w/v) formaldehyde solution for 1 h at room temperature, followed by washing three times with HBSS. The fibers were permeabilized with 0.3% (w/v) Triton-X 100 in HBSS for 30 min and then placed into a blocking buffer of 5% (w/v) BSA and 0.3% (w/v) Triton-X 100 solution for 1 h. Cardiac troponin T primary antibody solution was prepared by dilution into 1% (w/v) BSA solution (1:200), and the fibers were incubated in this solution at 4 °C overnight. The fibers were further placed into 1% (w/v) BSA solution containing donkey anti-rabbit-Alexa Fluor 488 secondary antibody (1:400) and Phalloidin iFlour 594 (1:1000) for 1 h. After three times washing with HBSS, the counterstaining for nuclei was performed with DAPI solution (1:1000) for 10 min. The fibers were washed three times with HBSS, and confocal imaging was done with SP8-DLS Leica microscope.

4.3.27. Metabolic activity assay of encapsulated cells
A Prestoblue assay (Invitrogen, A13261), was used to evaluate the proliferation of cells over time. Cell-laden fibers were cut into 5 mm sections with a razor blade which were carefully transferred into a 96 well plate where they were cultured in complete media. At each timepoint (1 d, 2 d), the fiber sections were transferred to fresh wells containing 110 μl Prestoblue working solution (10% (v/v) Prestoblue reagent in media). After a 1 h incubation at 37 °C, 100 μl was transferred from each well to a separate plate and read on a microplate reader (560/590 nm ex/em). Cell-laden fibers were washed with media then returned to culture.

4.3.28. CMs beating observation
After 5 d of culture, the beating of CM-encapsulated fibers was recorded by EVOS M5000 digital inverted microscope (Thermo Fisher Scientific, Waltham, USA).

Data availability statement

The data that support the findings of this study are available upon reasonable request from the authors.

Acknowledgments

M A acknowledges the support from the Natural Sciences and Engineering Research Council of Canada (NSERC, RGPIN-2016-04024) and the Canadian Foundation for Innovation (35570) and the B C Knowledge Development Fund (BCKDF). H S acknowledges the support received from the Natural Sciences and Engineering Research Council of Canada (NSERC) (NSERC, RGPIN-2021-03960, DGECR-2021-00337)Fonds de Recherche du Québec Santé (FRQS) (Chercheurs-boursiers J1 (313837) and Establishment of Young Investigators (324277), and Montreal TransMedTech Institute (iTMT). M A and E P thank support received from the Canadian Institutes for Health Research (CIHR, 201610PJT). A M acknowledges the Merit Scholarship of the Faculty of Medicine of the University of Montreal. M A and A K acknowledge the support received from Terasaki Institute for Biomedical Innovation.

ORCID iDs

Amir Seyfoori https://orcid.org/0000-0001-7745-2396
Mahmood Razzaghi https://orcid.org/0000-0002-3466-4206
Ali Khademhosseini https://orcid.org/0000-0002-2692-1524
Houman Savoji https://orcid.org/0000-0002-5596-673X
Mohsen Akbari https://orcid.org/0000-0003-2902-6557

References

[1] Murphy S V and Atala A 2014 3D bioprinting of tissues and organs *Nat. Biotechnol.* **32** 773
Lee A, Hudson A, Shiwarski D, Tashman J, Hinton T, Yerneni S, Bliley J, Campbell P and Feinberg A 2019 3D bioprinting of collagen to rebuild components of the human heart *Science* **365** 482–7
Grigoryan B *et al* 2019 Multivascular networks and functional intravascular topologies within biocompatible hydrogels *Science* **364** 458

[2] Akbari M and Khademhosseini A 2022 Tissue bioprinting for biology and medicine *Cell* **185** 2644
[3] Richbourg N R, Peppas N A and Sikavitsas V I 2019 Tuning the biomimetic behavior of scaffolds for regenerative medicine through surface modifications *J. Tissue Eng. Regen. Med.* **13** 1275
[4] Matai I, Kaur G, Seyedsalehi A, McClinton A and Laurencin C T 2020 Progress in 3D bioprinting technology for tissue/organ regenerative engineering *Biomaterials* **226** 119536
Tavakol D N, Fleischer S and Vunjak-Novakovic G 2021 Harnessing organs-on-a-chip to model tissue regeneration *Cell Stem Cell* **28** 993
[5] Bhattacharyya A, Janarthanan G, Tran H N, Ham H J, Yoon J and Noh I 2021 Bioink homogeneity control during 3D bioprinting of multicomponent micro/nanocomposite hydrogel for even tissue regeneration using novel twin screw extrusion system *Chem. Eng. J.* **415** 128971
[6] Zhang Y, Dong Z, Li C, Du H, Fang N X, Wu L and Song Y 2020 Continuous 3D printing from one single droplet *Nat. Commun.* **11** 1
[7] Angelopoulos I, Allenby M C, Lim M and Zamorano M 2020 Engineering inkjet bioprinting processes toward translational therapies *Biotechnol. Bioeng.* **117** 272
[8] Sun H, Jia Y, Dong H, Dong D and Zheng J 2020 Combining additive manufacturing with microfluidics: an emerging method for developing novel organs-on-chips *Curr. Opin. Chem. Eng.* **28** 1
[9] Yu C, Schimelman J, Wang P, Miller K L, Ma X, You S, Guan J, Sun B, Zhu W and Chen S 2020 Photopolymerizable biomaterials and light-based 3D printing strategies for biomedical applications *Chem. Rev.* **120** 10695
[10] Park J H, Jang J, Lee J-S and Cho D-W 2017 Three-dimensional printing of tissue/organ analogues containing living cells *Ann. Biomed. Eng.* **45** 180
Harley W S , Li C C, Toombs J, O'Connell C D, Taylor H K, Heath D E and D J Collins 2021 Advances in biofabrication techniques towards functional bioprinted heterogeneous engineered tissues: a comprehensive review *Bioprinting* **23** e00147
Williams D, Thayer P, Martinez H, Gatenholm E and Khademhosseini A 2018 A perspective on the physical, mechanical and biological specifications of bioinks and the development of functional tissues in 3D bioprinting *Bioprinting* **9** 19
Fang Y, Sun W, Zhang T and Xiong Z 2022 Recent advances on bioengineering approaches for fabrication of functional engineered cardiac pumps: a review *Biomaterials* **280** 121298
Duarte Campos D F and De Laporte L 2021 Digitally fabricated and naturally augmented *in vitro* tissues *Adv. Healthcare Mater.* **10** 2001253
[11] Yan Q, Dong H, Su J, Han J, Song B, Wei Q and Shi Y 2018 A review of 3D printing technology for medical applications *Engineering* **4** 729
Ravnic D J, Leberfinger A N, Koduru S V, Hospodiuk M, Moncal K K, Datta P, Dey M, Rizk E and Ozbolat I T 2017 Transplantation of bioprinted tissues and organs: technical and clinical challenges and future perspectives *Ann. Surg.* **266** 48
[12] Ashammakhi N, Ahadian S, Pountos I, Hu S-K, Tellisi N, Bandaru P, Ostrovidov S, Dokmeci M R and Khademhosseini A 2019 *In situ* three-dimensional printing for reparative and regenerative therapy *Biomed. Microdevices* **21** 42
Kahin K, Khan Z, Albagami M, Usman S, Bahanshal S, Alwazani H, Majid M, Rauf S and Hauser C 2019 Development of a robotic 3D bioprinting and microfluidic pumping system for tissue and organ engineering *Proc. SPIE* **10875** 108750Q
[13] Singh S, Choudhury D, Yu F, Mironov V and Naing M W 2020 *In situ* bioprinting—bioprinting from benchside to bedside? *Acta Biomater.* **101** 14
Chouhan D, Dey N, Bhardwaj N and Mandal B B 2019 Emerging and innovative approaches for wound healing and skin regeneration: current status and advances *Biomaterials* **216** 119267
Pazhouhnia Z, Beheshtizadeh N, Namini M S and Lotfibakhshaiesh N 2022 Portable hand-held bioprinters promote in situ tissue regeneration *Bioeng. Trans. Med.* **7** e10307
[14] O'Connell C D *et al* 2016 Development of the Biopen: a handheld device for surgical printing of adipose stem cells at a chondral wound site *Biofabrication* **8** 015019
[15] Ying G, Manríquez J, Wu D, Zhang J, Jiang N, Maharjan S, Hernández Medina D H and Zhang Y S 2020 An open-source handheld extruder loaded with pore-forming bioink for *in situ* wound dressing *Mater. Today Bio* **8** 100074
[16] Duchi S *et al* 2017 Handheld co-axial bioprinting: application to *in situ* surgical cartilage repair *Sci. Rep.* **7** 5837
[17] Nuutila K, Samandari M, Endo Y, Zhang Y, Quint J, Schmidt T A, Tamayol A and Sinha I 2022 *In vivo* printing of growth factor-eluting adhesive scaffolds improves wound healing *Bioact. Mater.* **8** 296
[18] Quint J P *et al* 2021 *In vivo* printing of nanoenabled scaffolds for the treatment of skeletal muscle injuries *Adv. Healthcare Mater.* **10** e2002152
[19] Hakimi N, Cheng R, Leng L, Sotoudehfar M, Ba P Q, Bakhtyar N, Amini-Nik S, Jeschke M G and Günther A 2018 Handheld skin printer: *in situ* formation of planar biomaterials and tissues *Lab Chip* **18** 1440
[20] Miri A K *et al* 2018 Microfluidics-enabled multimaterial maskless stereolithographic bioprinting *Adv. Mater.* **30** 1800242
[21] Dabiri S M H *et al* 2021 Multifunctional thermoresponsive microcarriers for high-throughput cell culture and enzyme-free cell harvesting *Small* **17** 2103192
[22] Mirani B, Stefanek E, Godau B, Hossein Dabiri S M and Akbari M 2021 Microfluidic 3D printing of a photo-cross-linkable bioink using insights from computational modeling *ACS Biomater. Sci. Eng.* **7** 3269
[23] Ouyang L, Highley C B, Sun W and Burdick J A 2017 A generalizable strategy for the 3D bioprinting of hydrogels from nonviscous photo-crosslinkable inks *Adv. Mater.* **29** 1604983
[24] Liu W, Zhong Z, Hu N, Zhou Y, Maggio L, Miri A K, Fragasso A, Jin X, Khademhosseini A and Zhang Y S 2018 Coaxial extrusion bioprinting of 3D microfibrous constructs with cell-favorable gelatin methacryloyl microenvironments *Biofabrication* **10** 024102
[25] Mironi-Harpaz I, Wang D Y, Venkatraman S and Seliktar D 2012 Photopolymerization of cell-encapsulating hydrogels: crosslinking efficiency versus cytotoxicity *Acta Biomater.* **8** 1838
[26] Cui X, Breitenkamp K, Finn M, Lotz M and D'Lima D D 2012 Direct human cartilage repair using three-dimensional bioprinting technology *Tissue Eng.* A **18** 1304
[27] Wang Z, Jin X, Dai R, Holzman J F and Kim K 2016 An ultrafast hydrogel photocrosslinking method for direct laser bioprinting *RSC Adv.* **6** 21099
[28] Fedorovich N E, Oudshoorn M H, van Geemen D, Hennink W E, Alblas J and Dhert W J 2009 The effect of photopolymerization on stem cells embedded in hydrogels *Biomaterials* **30** 344
Pereira R F and Bártolo P J 2015 3D bioprinting of photocrosslinkable hydrogel constructs *J. Appl. Polym. Sci.* **132**
[29] Dasari S, Fang Y and Mitra A K 2018 Cancer associated fibroblasts: naughty neighbors that drive ovarian cancer progression *Cancers* **10** 406
[30] Novosel E C, Kleinhans C and Kluger P J 2011 Vascularization is the key challenge in tissue engineering. *Adv. Drug Deliv. Rev.* **63** 300
[31] Mirani B, Pagan E, Currie B, Siddiqui M A, Hosseinzadeh R, Mostafalu P, Zhang Y S, Ghahary A and Akbari M 2017 An advanced multifunctional hydrogel-based dressing for

wound monitoring and drug delivery *Adv. Healthcare Mater.* **6** 1700718

[32] Han L, Lu X, Wang M, Gan D, Deng W, Wang K, Fang L, Liu K, Chan C W and Tang Y 2017 A mussel-inspired conductive, self-adhesive, and self-healable tough hydrogel as cell stimulators and implantable bioelectronics *Small* **13** 1601916
Mehrali M, Bagherifard S, Akbari M, Thakur A, Mirani B, Mehrali M, Hasany M, Orive G, Das P and Emneus J 2018 Blending electronics with the human body: a pathway toward a cybernetic future *Adv. Sci.* **5** 1700931
Mirani B, Pagan E, Shojaei S, Dabiri S M H, Savoji H, Mehrali M, Sam M, Alsaif J, Bhiladvala R B and Dolatshahi-Pirouz A 2020 Facile method for fabrication of meter-long multifunctional hydrogel fibers with controllable biophysical and biochemical features *ACS Appl. Mater. Interfaces* **12** 9080

[33] Esmaeili H, Patino-Guerrero A, Hasany M, Ansari M O, Memic A, Dolatshahi-Pirouz A and Nikkhah M 2021 Electroconductive biomaterials for cardiac tissue engineering *Acta Biomater.* **139** 118–40
Distler T and Boccaccini A R 2020 3D printing of electrically conductive hydrogels for tissue engineering and biosensors—a review *Acta Biomater.* **101** 1

[34] Samimi Gharaie S, Seyfoori A, Khun Jush B, Zhou X, Pagan E, Godau B and Akbari M 2021 Silicate-based electro-conductive inks for printing soft electronics and tissue engineering *Gels* **7** 240